# Photon Absorption of Two-dimensional Nonsymmorphic Dirac Semimetals

Amarnath Chakraborty,[*] Guang Bian, and Giovanni Vignale[†]

*Department of Physics and Astronomy,*

*University of Missouri, Columbia, Missouri, USA*

(Dated: March 18, 2022)

## Abstract

Two-dimensional Dirac semimetals have attracted a great deal of attention because of their linear energy dispersion and non-trivial Berry phase. These materials are rare because the nodal band structure is fragile against perturbations such as the spin-orbit coupling (SOC). Recently, it has been reported that nonsymmorphic crystal lattices possess symmetry-enforced Dirac-like band dispersion around certain high symmetry momenta even in the presence of SOC. Here we calculate the optical absorption spectra of the nonsymmorphic semimetals, which hosts anisotropic Dirac cones, with different Fermi velocities along the $x$ and $y$ directions. Our calculations show that the optical absorption coefficient depends strongly on the anisotropy factor and the photon polarization. By rotating the latter, one can change the absorption coefficient by more than an order of magnitude, giving rise to *birefringence*. When a magnetic field is applied, the absorption coefficient also depends on an internal parameter, which we term the "mixing angle" of the band structure. This parameter becomes therefore accessible to experimental investigation. We further find that an in-plane magnetic field, while leaving the system gapless, can induce a Van-Hove singularity in the joint density of states: this causes a significant enhancement of the optical absorption at the frequency of the singularity for one direction of polarization but not for the orthogonal one, making the optical properties even more strongly dependent on polarization and anisotropy. These results suggest that a very pure nonsymmorphic 2D Dirac semimetal can be an excellent candidate material for tunable magneto-optic devices.

Keywords: Non-symmorphic, *birefringence*, Optical absorption coefficient

---

[*] achakraborty@mail.missouri.edu

[†] vignaleg@missouri.edu

# I. INTRODUCTION

Over the past decade, two-dimensional (2D) Dirac-like electron gases have attracted tremendous research interest, with examples ranging from graphene [1] to topological insulators [2] to Dirac and Weyl semimetals. These materials [3–5] possess several unique electronic and optical properties traceable to their linear energy dispersion and non-trivial Berry phase. Graphene has become the prototypical instance of two-dimensional Dirac fermions. However, the Dirac points in many existing 2D materials, including graphene, are vulnerable to spin-orbit coupling (SOC). Motivated by finding alternative 2D materials beyond graphene, various atomically thin materials, including silicene, germanene, few-layer black phosphorus, and other 2D compounds, have been theoretically proposed and experimentally prepared [6–9]. Recently, symmetry-protected 2D Dirac semimetals have attracted intense interest. These materials feature Dirac points that are not gapped by SOC interaction and are protected by nonsymmorphic lattice symmetry [10, 11].

Dirac-like band dispersions have recently been observed in the nonsymmorphic monolayer film, $\alpha$-bismuthene [11]. The lattice structure of $\alpha$-bismuthene belongs to the #42 layer group (*pman*), as shown in Fig. 1(a). There are two atomic sublayers marked by 'A' and 'B' in $\alpha$-bismuthene with a vertical spacing of 3.02 Å in between. The in-plane lattice constants are 4.53 and 4.72 Å in the $x$ and $y$ directions, respectively. The lattice is invariant under a glide mirror reflection. That is a mirror reflection to the middle plane between the two sublayers followed by a translation by a half lattice constant in both $x$ and $y$ directions. This nonsymmorphic glide mirror symmetry leads to band degeneracy at the high symmetry momentum points $\bar{X}_1$ and $\bar{X}_2$ of the Brillouin zone, see Fig. 1(b). The first-principles band structure (Fig. 1(c)) indeed exhibits band crossing features among all the bands at $\bar{X}_1$ and $\bar{X}_2$. The top Dirac nodes in valence bands $\bar{X}_1$ and $\bar{X}_2$ are denoted by 'DP1' and 'DP2', respectively. The two Dirac nodes are not connected by any lattice symmetry operation. Therefore, they are at different energies: DP1 at 0.7 eV and DP2 and 0.4 eV. Though the two nodes are not at the Fermi level in the pristine material, their energies can be shifted by applying a gating voltage and/or a strain. Another example of nonsymmorphic symmetry leading to protected Dirac points is found in Bi monolayer ([11]; see the section VII of the supplementary information [12] Fig S4), with layer group LG-p21/m11 (screw axis), where the Dirac points are predicted to be much closer to the Fermi level.

To effectively optimize and utilize the unique properties of 2D materials, various strategies
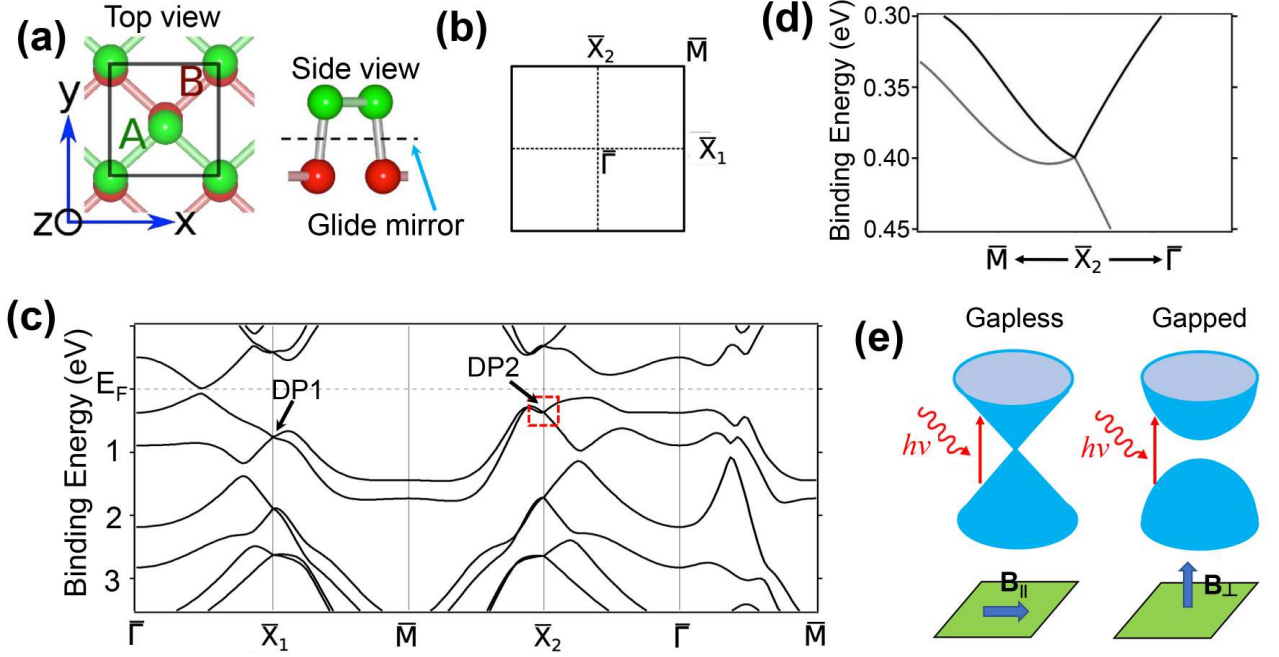
Figure 1: **(a)** Lattice structure of $\alpha$-bismuthene. **(b)** Brillouin zone of $\alpha$-bismuthene where $\bar{X}_1$ $(\pi, 0)$ and $\bar{X}_2$ $(0, \pi)$ are the two Dirac points (DP). **(c)** Band structure of $\alpha$-bismuthene. This shows both DPs are below Fermi energy. The Fermi velocities are $v_x = 3.95 \times 10^5$ $m/s$ and $v_y = 2.12 \times 10^5$ $m/s$ at DP1, and $v_x = 1.19 \times 10^5$ $m/s$ and $v_y = 4.67 \times 10^5$ $m/s$ at DP2. **(d)** Zoom-in band structure marked by the red box in (c), emphaiszing the strong anisoptrpy present in DP2 $(\bar{X}_2)$. **(e)** The band is gapped in case the direction of magnetic field is normal to the plane and gapless for parallel to the plane.

have been proposed to tune the optical and electronic properties, such as the introduction of electric fields, strain modulation [13, 14], atom doping [15], strain engineering [16], etc. However, to date, the optical properties of 2D nonsymmorphic Dirac materials have not been systematically investigated [17–19].

There are two crucial differences between nonsymmorphic Dirac semimetals and graphene-like 2D Dirac materials. First, an anisotropy factor $\rho$ is allowed by the lower symmetry of the system. Our calculations show that $\rho$ plays a vital role in controlling photon absorption. Second, the spin (the $\sigma$ matrices) and orbital (the $\tau$ matrices) degrees of freedom are coupled together in our model Hamiltonian. Therefore, nonsymmorphic Dirac semimetals support strong spin-orbit coupling, unlike graphene, in which the spin and orbital parts are largely decoupled. These two facts yield a richer spectrum of optical properties in nonsymmorphic Dirac semimetals than in graphene, in

particular a great sensitivity to the application of a magnetic field as discussed below.

In this paper, we will investigate the new features that nonsymmorphic symmetry brings to the optical absorption spectrum. Thus, we will assume that at least one nonsymmorphic Dirac node is present at the Fermi level and is directly accessible to photon absorption processes. Our model for nonsymmorphic 2D Dirac cone is spelled out in Eq. (3) and we will examine the role played by the intrinsic parameters of that model, i.e., the "anisotropy factor" and the "mixing angle". While the Dirac cone is expected, under this assumption, to be the main contributor to the low-frequency optical absorption spectrum, it is not possible, in general, to completely eliminate low-frequency contributions from metallic regions of momentum space, where the Fermi level crosses partially occupied bands. This point will be addressed in detail in the concluding section, where we will argue that the residual metallic absorption can be clearly separated from Dirac-cone absorption in sufficiently clean samples, because it gives rise to a distinct Drude absorption peak.

We perform our calculations without and with the magnetic field, and in the latter case, we consider three orthogonal directions of the field. We find that a magnetic field perpendicular to the plane opens a gap in the spectrum. The magnitude of this gap can be related to the internal "mixing angle" – a quantity not directly accessible from the band structure in the absence of a magnetic field. On the other hand, an in-plane magnetic field leaves the system gapless but splits the Dirac nodes. For one direction of the magnetic field, a Van-Hove singularity appears in the joint density of states. It is associated with a change in the topology of the constant energy contours at a saddle point in the band structure. The logarithmic divergence of the joint density of states leads to enhanced absorption for one direction of the photon polarization but not for the orthogonal one, which implies that the absorption coefficient is very sensitive to the polarization of the incident light when the frequency approaches the Van-Hove singularity.

One of our significant findings is that the absorption coefficient can be tuned by changing the polarization and frequency of the incoming wave. This tunability is further enhanced by the intrinsic anisotropy of the Dirac cones. These results open the door to interesting magneto-optical applications of 2D nonsymmorphic Dirac materials.

4

## II. MODEL AND SYMMETRIES

We have taken the example of $\alpha$-bismuthene as the nonsymmorphic material described in the reference [11]. According to this paper the Dirac cones exists at $\bar{X}_1 = (\pi, 0)$ and $\bar{X}_2 = (0, \pi)$ of the Brillouin zone. $\alpha$-Bi is nonmagnetic and centrosymmetric, so the time-reversal (T) and inversion (P) symmetries are preserved. The symmetries in this model can be described by the three generators:

$$\tilde{M}_z : (x + 1/2, y + 1/2, -z) \; i\sigma_z$$
$$P : (-x, -y, -z) \; \sigma_0 \tag{1}$$
$$M_x : (-x, y, z) \; i\sigma_x$$

Here, $\tilde{M}_z$ represents a nonsymmorphic glide mirror operation – the mirror reflection accompanied by a half lattice translation parallel to the mirror plane in the case of $\alpha$-bismuthene. In Eq. (3), x, y z are spatial coordinates while $\sigma_i$ are Pauli matrices for the spin degree of freedom. Equation (1) describes the action of symmetry operators on the spatial coordinates and spin space. It would instead represent a screw-axis symmetry in the case of monolayer Bi. We can write the matrix representation of the symmetry operators as

$$T = -i\sigma_y \otimes \tau_0 K \; \text{(Time reversal)}$$
$$\tilde{M}_z = \sigma_z \otimes \tau_y \; \text{(Glide mirror)}$$
$$P = \sigma_0 \otimes \tau_x \; \text{(Parity)} \tag{2}$$
$$M_x = -i\sigma_x \otimes \tau_x \; \text{(Mirror -x)},$$

where $K$ is the complex conjugation part which can be thought of a $2 \times 2$ matrix. Here, $\sigma_i$ $(i = x, y, z)$ are Pauli matrices for the spin and $\tau_i$ $(i = x, y, z)$ are the Pauli matrices for orbital degrees of freedom respectively and $\sigma_0$ and $\tau_0$ are the $2 \times 2$ identity matrix [11].

### A. Model Hamiltonian without magnetic field

For our purpose, we first consider the Dirac cone $\bar{X}_1 = (\pi, 0)$ where the Hamiltonian can be written as:

$$H = \rho v k_x (\cos\alpha \; \sigma_x \otimes \tau_z + \sin\alpha \; \sigma_0 \otimes \tau_y) + v k_y \; (\sigma_y \otimes \tau_z)$$
$$= \rho v k_x (\cos\alpha \; \gamma_z + \sin\alpha \; \gamma_x) + v k_y \gamma_y \; , \tag{3}$$

5

where $\gamma_z = \sigma_x \otimes \tau_z$, $\gamma_y = \sigma_y \otimes \tau_z$ and $\gamma_x = \sigma_0 \otimes \tau_y$. We define $\rho$ as the anisotropy factor $\rho = \frac{v_x}{v_y}$ because it refers to the mismatch in the Fermi velocity along $x$ and $y$-direction, where $v_y = v$ and $\rho v = v_x$. The angle $\alpha$ is what we termed the "mixing angle," which is an intrinsic parameter of the model as well.

The $\tilde{M}_z$ symmetry helps us to decompose the Hamiltonian into two $2\times2$ matrices representing the $\tilde{M}_z$ even sector (eigenvalue +1) and odd sector (eigenvalue -1). For convenience we chose the even sector to work with, corresponding to $\sigma_z = 1$, $\tau_y = 1$ and $\sigma_z = -1$, $\tau_y = -1$. Choosing a convenient basis (Please check the section I [12]) in the even sector we arrive at the reduced form of the Hamiltonian:

$$\tilde{H}_{\tilde{M}_z=1} = \rho v k_x(\sigma_x \cos \alpha \ + \sigma_y \sin \alpha) + v k_y \sigma_z, \tag{4}$$

The anisotropy factor $\rho$ is material-dependent. The two Dirac cones of bismuthene have different $\rho$ values, namely, $\rho = 1.86$ at $\bar{X}_1$ and $0.25$ at $\bar{X}_2$, because the two valleys are not connected by any crystal symmetries. In the following discussion, we will take $\rho$ as a free parameter of the model and study the $\rho$-dependence of optical absorption.

In both cases, the eigenvalues are respectively.

$$E = \pm v \sqrt{\rho^2 k_x^2 + k_y^2} \tag{5}$$

Notice that we could reduce the whole Hamiltonian to $2\times2$ form only because the system has the glide mirror symmetry $\tilde{M}_z$.

### B. Model Hamiltonian with Magnetic field

Introducing a magnetic field in this system reduces the symmetry. We go back to the original form of the Hamiltonian to find the eigenstates and eigenvectors. The Hamiltonian with the magnetic field is

$$\tilde{H} = \rho v k_x \big( \cos \alpha \ \gamma_z + \sin \alpha \ \gamma_x \big) + v k_y \gamma_y + \vec{B} \cdot \tau_0 \ \vec{\sigma}, \tag{6}$$

The direction of the magnetic field is described by polar ($\mu$) and azimuthal angles ($\nu$) such that

$$\vec{B} = B \left( \sin \mu \cos \nu, \sin \mu \sin \nu, \cos \mu \right), \tag{7}$$

We also set

$$v \rho k_x = \bar{k} \cos \phi \,, \qquad v k_y = \bar{k} \sin \phi \,. \tag{8}$$

6

With this notation the energy eigenvalues are [1]

$$\bar{E}(\phi) = \pm\sqrt{B^2 + \bar{k}^2 \pm 2B\bar{k}F(\phi)}\,, \tag{9}$$

where

$$F(\phi) = \sqrt{(\cos\phi\cos\alpha)^2 + \sin^2\mu(\cos\phi\cos\nu\sin\alpha + \sin\phi\sin\nu)^2}\,, \tag{10}$$

The spectrum is generally gapped in presence of magnetic field. We find the band gap $\Delta$ using Eq. (9) as:

$$\frac{\Delta}{B} = 2\min\frac{|\bar{E}(\phi)|}{B} = 2\sqrt{1 - \frac{A + C + \sqrt{A^2 + C^2 + 2AC\cos(2\gamma)}}{2}}\,, \tag{11}$$

where we have defined

$$\cos(2\gamma) = \frac{\sin^2\alpha - \tan^2\nu}{\sin^2\alpha + \tan^2\nu}\,, \tag{12}$$

and

$$A = \cos^2\alpha\,, \quad C = \sin^2\mu(\cos^2\nu\sin^2\alpha + \sin^2\nu). \tag{13}$$

In the special case of magnetic field along the $z$-axis ($\mu = 0$), we get $A = \cos^2\alpha$, $C = 0$, $\frac{\Delta}{B} = 2\sin\alpha$.

If the magnetic field is along the $x$-axis ($\mu = \pi/2, \nu = 0$), we have $A = \cos^2\alpha$, $C = \sin^2\alpha$, $\cos(2\gamma) = 1$, yielding $\Delta = 0$.

If the magnetic field is along the $y$-axis ($\mu = \pi/2, \nu = \pi/2$), we have $A = \cos^2\alpha$, $C = 1$, $\cos(2\gamma) = -1$, yielding $\Delta = 0$.

The bandgap along $z$-direction of field depends on the mixing angle $\alpha$. Thus, by measuring the bandgap in the presence of a magnetic field one can determine the value of the mixing angle.

## III. MATHEMATICAL FRAMEWORK TO CALCULATE THE OPTICAL ABSORPTION COEFFICIENT

The electromagnetic interaction is given by $\vec{J} \cdot \vec{A}(t)$, where $\vec{J} = \frac{\partial H}{\partial\vec{k}}$ is the current operator with components

$$J_x = \rho v(\cos\alpha\ \sigma_x \otimes \tau_z + \sin\alpha\ \sigma_0 \otimes \tau_y)\,, \quad J_y = v\tau_z\sigma_y\,. \tag{14}$$

---

[1] Notice that the eigenvalues come in pairs of opposite sign. This is because the original Hamiltonian anticommutes with the operator $\tau_z\boldsymbol{\sigma} \cdot (\tilde{\mathbf{k}} \times \mathbf{B})$ where $\tilde{\mathbf{k}}$ is a vector with components $(k_x\sin\alpha, k_y, 0)$.

and $\vec{A}(t)$ is the vector potential

$$\vec{A}(t) = A_0 \cos(\omega t) \, \mathbf{e}, \tag{15}$$

where $A_0$ is the amplitude of the electromagnetic wave and the polarization vector $\mathbf{e}$ is defined as. [2]

$$\mathbf{e} = \cos \beta \hat{\mathbf{x}} + e^{i\delta} \sin \beta \hat{\mathbf{y}} \tag{16}$$

The optical transition probability is

$$W_{v \to c}(\omega) = \frac{A^2 v^2}{2\pi \hbar} \sum_j \int_0^\infty d\bar{k} \bar{k} \int_{\phi_{\min}}^{\phi_{\max}} d\phi \, |M_j(\phi)|^2 \frac{\delta(\bar{k} - \bar{k}_j(\phi))}{|d(E_c - E_v)(\bar{k}, \phi)/d\bar{k}|}, \tag{17}$$

where $\bar{k}_j(\phi)$, with $j = +$ or $-$ are the constant energy contours at the transition energy $\omega$, i.e., the solutions of the equation $E_c(\bar{k}, \phi) - E_v(\bar{k}, \phi) = 2\hbar\omega$, and $v \to c$ refers to the transition from the valence band to the conduction band. The squared matrix element of the current operator is given by

$$|M_j(\phi)|^2 \equiv \left| \langle \psi_{cj}(\phi) | \rho^{1/2} \, \cos \beta \, J_x + e^{-i\delta} \rho^{-1/2} \, \sin \beta \, J_y | \psi_{vj}(\phi) \rangle \right|^2, \tag{18}$$

where

$$|\psi_{vj}(\phi)\rangle \equiv |\psi_v(\bar{k}_j(\phi), \phi)\rangle, \quad |\psi_{cj}(\phi)\rangle \equiv |\psi_c(\bar{k}_j(\phi), \phi)\rangle. \tag{19}$$

are, respectively, the valence and conduction band states evaluated at the iso-energy surface, i.e., $\bar{k} = \bar{k}_j(\phi)$. From Eq. (17) we have an expression for the transition probability that we can utilize to calculate the optical absorption from different pairs of bands (e.g, $v_1 \to c_1$ or $v_1 \to c_2$), with or without the magnetic field.

For example, if we consider only intra-valley transition $v_1 \to c_1$ we find that the transition probability is

$$W_{v1 \to c1}(\omega) = \frac{A^2 \omega}{2\pi \hbar} \int_{\phi_{\min}}^{\phi_{\max}} d\phi \frac{k_+(\phi)|M_+(\phi)|^2 + k_-(\phi)|M_-(\phi)|^2}{\sqrt{F(\phi)^2 + \left(\frac{\omega}{2}\right)^2 - 1}}, \tag{20}$$

where $\omega$ is the excitation energy and has value $\Delta < \omega < 2B$ ($\Delta$ is the bandgap of the system). Here $\phi_{\min}$ and $\phi_{\max}$ are the lower and upper limits of integration, defined by the solutions of the equation

$$F(\phi)^2 = 1 - \left(\frac{\omega}{2}\right)^2. \tag{21}$$

---

[2] We are working in low energy regime thus using the dipole approximation and neglecting the photon momentum.

The two branches of the energy contours $\bar{k}_\pm(\phi)$ coincide at $\phi_{\min}$ and $\phi_{\max}$ and thus combine to produce closed contours around the minimum excitation energy (Look into the supplementary material section III [12] for calculation of the iso-energy contours).

## IV.   RESULTS AND DISCUSSIONS

Based on the mathematical framework described before, we can calculate the optical absorption coefficient for a general direction polarization with and without the magnetic field. First, we start with the case where there is no magnetic field in our system, and later we introduce a magnetic field in different directions.

### A.   Optical absorption coefficient without the magnetic field

In this case, as there is no magnetic field present, we have used the reduced Hamiltonian Eq. (4) for $\tilde{M}_z = +1$. The glide mirror symmetry holds for this case and has distinct eigenvalues for the two valleys ($\tilde{M}_z = \pm 1$), which prevents inter-valley transitions. As a result, we end up with only intra-valley transitions (i.e., $v_1 \to c_1$ or $v_2 \to c_2$ which are exactly equal). For the valley $\bar{X}_1$, we get the transition probability

$$W_{v1 \to c1} = \frac{A^2 \omega}{8} \Big( \rho \, \cos^2 \beta + \rho^{-1} \sin^2 \beta \Big), \tag{22}$$

The optical absorption coefficient calculated [20] for general direction of polarization without magnetic field takes the form:

$$\eta = \frac{\pi e^2}{2 \hbar c} f(\rho, \beta) \,, \tag{23}$$

where we have defined the *birefringence* function

$$f(\rho, \beta) = \big( \rho \, \cos^2 \beta \, + \, \rho^{-1} \, \sin^2 \beta \big) \,. \tag{24}$$

We have reinstated the $\hbar$ in order to get the dimensionless quantity, the fine structure constant ($\frac{e^2}{\hbar c} = 1/137$). This expression of optical absorbance is calculated for a single valley (which in the case of $\alpha$-bismuthene could be either the $\bar{X}_1$ or the $\bar{X}_2$ valley) as a function of the anisotropy factor $\rho$. It is also evident that this result is very similar to the well-known result for graphene, [3]

---

[3] The absorbance for monolayer graphene is $\eta_{graphene} = \frac{\pi e^2}{\hbar c}$.

in that the absorption coefficient is frequency-independent, but now it has a strong dependence on polarization, as indicated by the *birefringence* function. For large anisotropy ($\rho \ll 1$ or $\rho \gg 1$) the absorption coefficient can change by a significant factor upon rotating the polarization angle.

## B. Optical absorption coefficient in the presence of a magnetic field along the z-direction

When working with the magnetic field along the $z$-direction, the Zeeman term preserves the glide mirror symmetry; thus, we can still decouple the Zeeman term for even and odd sectors under the glide mirror symmetry operator. The Zeeman term $B\tau_0\sigma_z$ can be reduced to $B\sigma_z$ in the even sector and $-B\sigma_z$ in the odd sector. We have used the reduced Hamiltonian for the even sector of $\tilde{M}_z$ (Eq. (4)) and added the Zeeman term:

$$H'_{M_z=1} = (\rho v k_x \cos\alpha + B)\sigma_x \; + \; \rho v k_x \sin\alpha\sigma_y \; + \; v k_y\sigma_z \; , \tag{25}$$

We write the eigenvalues as

$$E = \pm v\sqrt{\left(\rho k_x + \frac{B}{v}\cos\alpha\right)^2 + k_y^2 + \frac{B^2}{v^2}\sin^2\alpha} \; . \tag{26}$$

From Fig. 2(a), we see the energy bands when the magnetic field is along the $z$-direction, and there exists a gap equals to $\Delta = 2B\sin\alpha$ (Eq. (11)), which means the bandgap has dependence over the intrinsic quantity "mixing angle".

Both the current operators $J_x$ and $J_y$ and our Hamiltonian (Eq. (25)) commutes with $\tilde{M}_z$, which makes the transitions preserve the parity of $\tilde{M}_z$. In Fig. 2(b), we have shown the two valleys have opposite symmetries against the glide mirror symmetry for the $z$-direction of the magnetic field, and hence inter-valley transitions are not allowed.

Calculations similar to the previous section for optical absorbance ($\eta_z$) for the $\bar{X}_1$ valley leads us to

$$\eta_z = \frac{\pi e^2}{2\hbar c}\left[f(\rho,\beta)(1 + \frac{4B^2}{\omega^2}\sin^2\alpha) + \frac{4B}{\omega}\sin\alpha\sin\delta\sin 2\beta\right] \; . \tag{27}$$

The *birefringence* function that appears in this expression will let us control the absorbance with the polarization of light. Also, it has a dependence on the frequency. For the $\bar{X}_2$ valley the expression is exactly the same with a different value for the anisotropy factor. To understand the
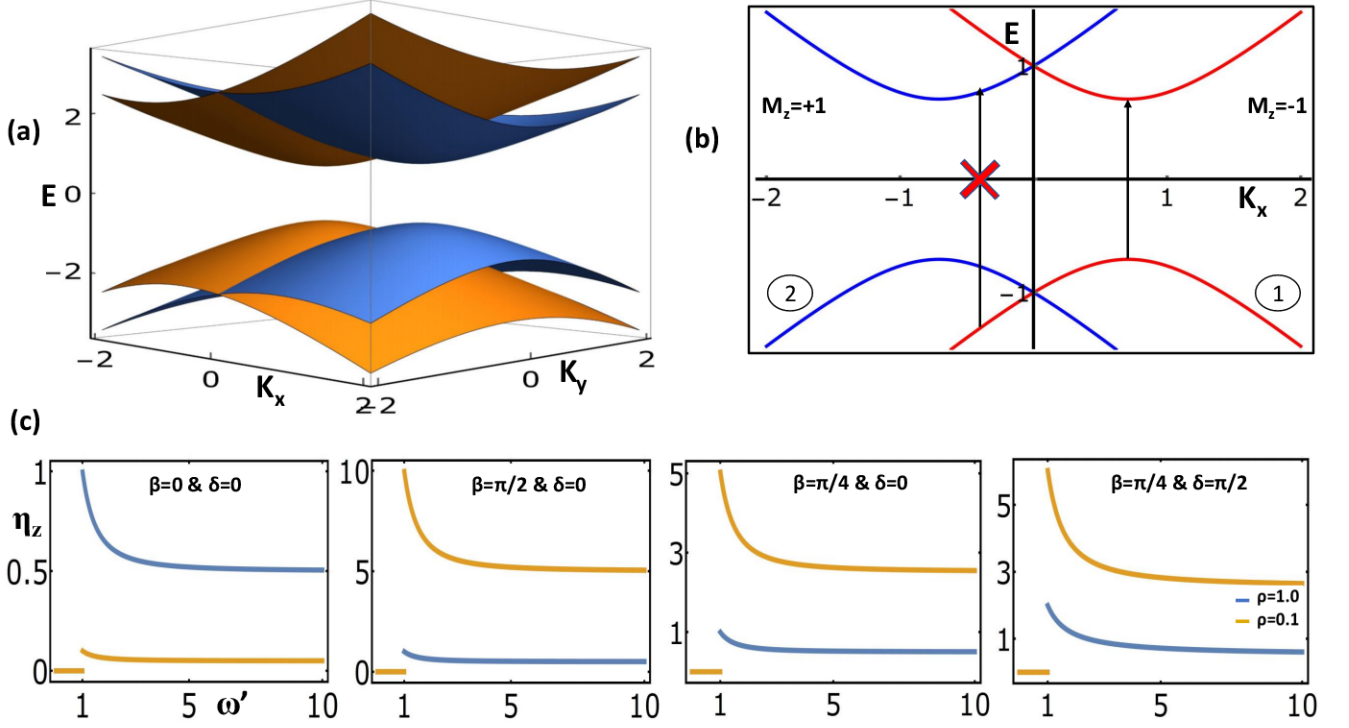
Figure 2: **(a)** Three-dimensional plot of the band dispersion for magnetic field in the $z$-direction. Notice that there is a band gap $\Delta = 2B \sin \alpha$ at two points separated by a wave vector proprtional to $B_z$ along $k_x$. The momenta $k_x$ and $k_y$ are in units of $\frac{B}{v}$ and the energy is in units of B. **(b)** This figure shows that only intra-valley transitions are possible as the two valleys hold opposite eigenvalues for $\tilde{M}_z$. **(c)** Plot of the optical absorption coefficient vs scaled frequency $\omega' = \frac{\omega}{2B \sin \alpha}$ for four different polarizations. The plot starts at $\omega \geq 2B \sin \alpha$.

effect of the anisotropy factor on the absorbance, we assumed one Dirac point to be nearly isotropic ($\rho \approx 1.0$) and the other Dirac point to be highly anisotropic ($\rho \approx 0.1$). In Fig. 2(c), we have plotted the optical absorption coefficient (Eq. 27) with frequency (scaled frequency $\omega' = \frac{\omega}{2B \sin \alpha}$) for both the isotropic and anisotropic Dirac points for four different polarization. From these figures, one can see when the polarization is along $x$-direction ($\beta = 0; \delta = 0$) (Fig. 2(c(i)) the dominating Dirac point is the isotropic one ($\rho = 1.0$) unlike the other cases where the the anisotropic ($\rho = 0.1$) case prevails in the absorption spectrum.

It shows when we change the polarization to the $x$-direction ($\beta = 0; \delta = 0$), we can significantly decrease the total absorbance, where if we switch to $y$-polarisation ($\beta = \pi/2; \delta = 0$) we increase the total absorption by an order of magnitude. This shows the Dirac point mainly contributing

11

to the enhancement of the absorbance is the anisotropic one, and this is due to the *birefringence* function present in the expression.

### C. Optical Absorption Coefficient in the presence of the Magnetic Field along the x-direction

For the magnetic field at $x$-direction, the Hamiltonian can be written as

$$H = \rho v k_x \, \cos\alpha \, \gamma_z + \rho v k_x \, \sin\alpha \, \gamma_x + v k_y \gamma_y + B_x \, \tau_0 \sigma_x \,, \tag{28}$$

The corresponding eigenvalues are:

$$E = \pm\sqrt{(\rho v k_x \pm B)^2 + v^2 k_y^2} \,, \tag{29}$$

From Fig. 3(a), we see that there is no bandgap, and the two valleys cross each other. Similarly to the $z$-direction, we find that a symmetry operator $\tau_y \sigma_x$ is present in this case, which commutes with the current operators and the Hamiltonian. This has opposite signs in the two valleys (shown Fig. 3(b)) and thus only allows intra-valley transitions for optical absorption. This symmetry operator $\tau_y \sigma_x$ (product of the two broken symmetries, time reversal, and glide mirror) protects Dirac cones even though time-reversal symmetry is broken due to the presence of the magnetic field.

For each valley, we get the optical absorption coefficient in the form:

$$\eta_x = \frac{\pi e^2}{2\hbar c} \, f(\rho, \beta) \,, \tag{30}$$

which coincides with the result obtained with no magnetic field.

### D. Optical absorption coefficient in the presence of a magnetic field in the y-direction

For a magnetic field in the $y$-direction, the Hamiltonian can be written as

$$H = \rho v k_x \cos\alpha\gamma_z + \rho v k_x \sin\alpha\gamma_x + v k_y \gamma_y + B_y \tau_0 \sigma_y \,, \tag{31}$$

where the $\gamma$ matrices are defined after Eq. (3). Its eigenvalues are

$$E = \pm\sqrt{\left(\sqrt{(\rho v k_x \cos\alpha)^2 + (v k_y)^2} \pm B\right)^2 + \left(\rho v k_x \sin\alpha\right)^2} \,. \tag{32}$$
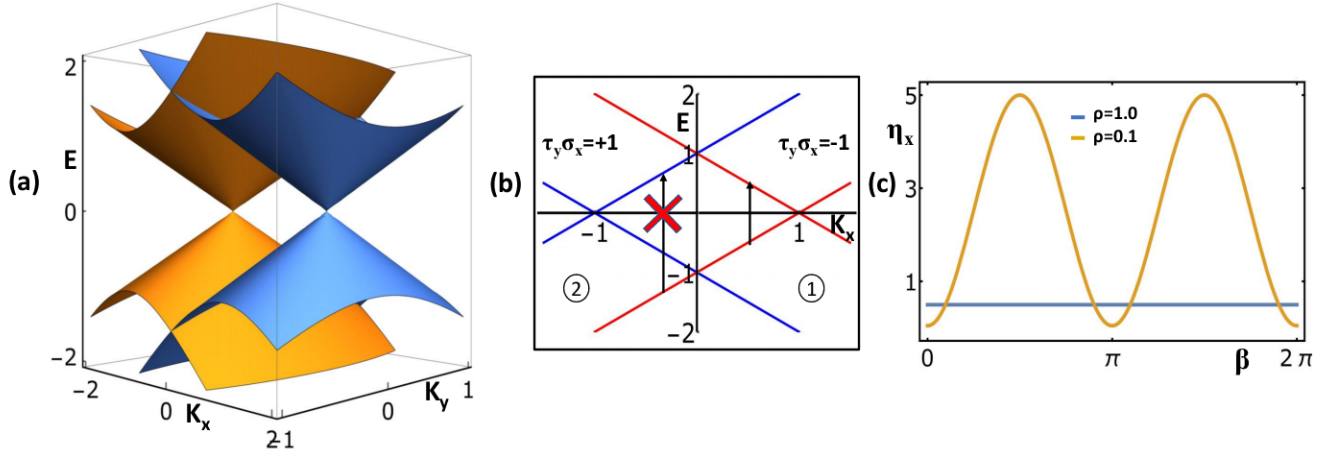
Figure 3: **(a)** Three-dimensional plot of the energy bands for magnetic field along the $x$-direction. The spectrum is gapless. **(b)** This figure shows that only intra-valley transitions are possible as the two valleys hold opposite eigenvalues of $\tau_y \sigma_x$. **(c)** Plot of the absorption coefficient $\eta_x$ vs $\beta$ for $\alpha = \pi/4$, for two different values of $\rho$, referring to the isotropic ($\rho = 1.0$) and the anisotrpic ($\rho = 0.1$) valley respectively. The absorption coefficient is in a unit of $\eta_{grahene}$.

Let us start our calculation for the magnetic field in $y$-direction by keeping $\rho = 1$ (isotropic valley). This means that the only source of anisotropy is the magnetic field itself. From Fig. 4(a) we see that the Dirac point, which initially was at $\bar{X}_1$, is split by the magnetic field term $B\tau_0\sigma_y$ into two distinct Dirac points located at $k_x = 0$, $k_y = \pm B/v$. The two Dirac points are related to each other by parity symmetry ($\sigma_0 \tau_x$ combined with the inversion of $\mathbf{k}$), which remains intact in this case. The bands emanating from the two Dirac cones (depicted in blue in Fig. 4(a)) account for the low-frequency part of the absorption spectrum. The high and low energy bands, depicted in orange in Fig. 4(a), become degenerate with the blue bands at the $\bar{X}_1$ point ($k_x = k_y = 0$), as required by parity symmetry. Also, this band dispersion gives rise to a saddle point at $k_x = \cos\alpha, k_y = 0$ as can be directly verified from Eq. (32). The singularity occurs in the "blue" bands, and the transition frequency associated with it is $\omega_{\text{critical}} = 2B\sin\alpha$.

We performed numerical calculations for the absorption coefficient in the presence of a magnetic field along the $y$-direction. There is no selection rule from the symmetry constraints in this case. Thus we have included all the possible transitions (inter-valley transitions i.e., $v_1 \rightarrow c_2$ together with intra-valley transitions i.e., $v_1 \rightarrow c_1$) and obtained the optical absorption coefficient as shown in Fig. 4(d). Notice that we only have intra-valley transitions for $\omega \leq 2B$. For $\omega \geq 2B$
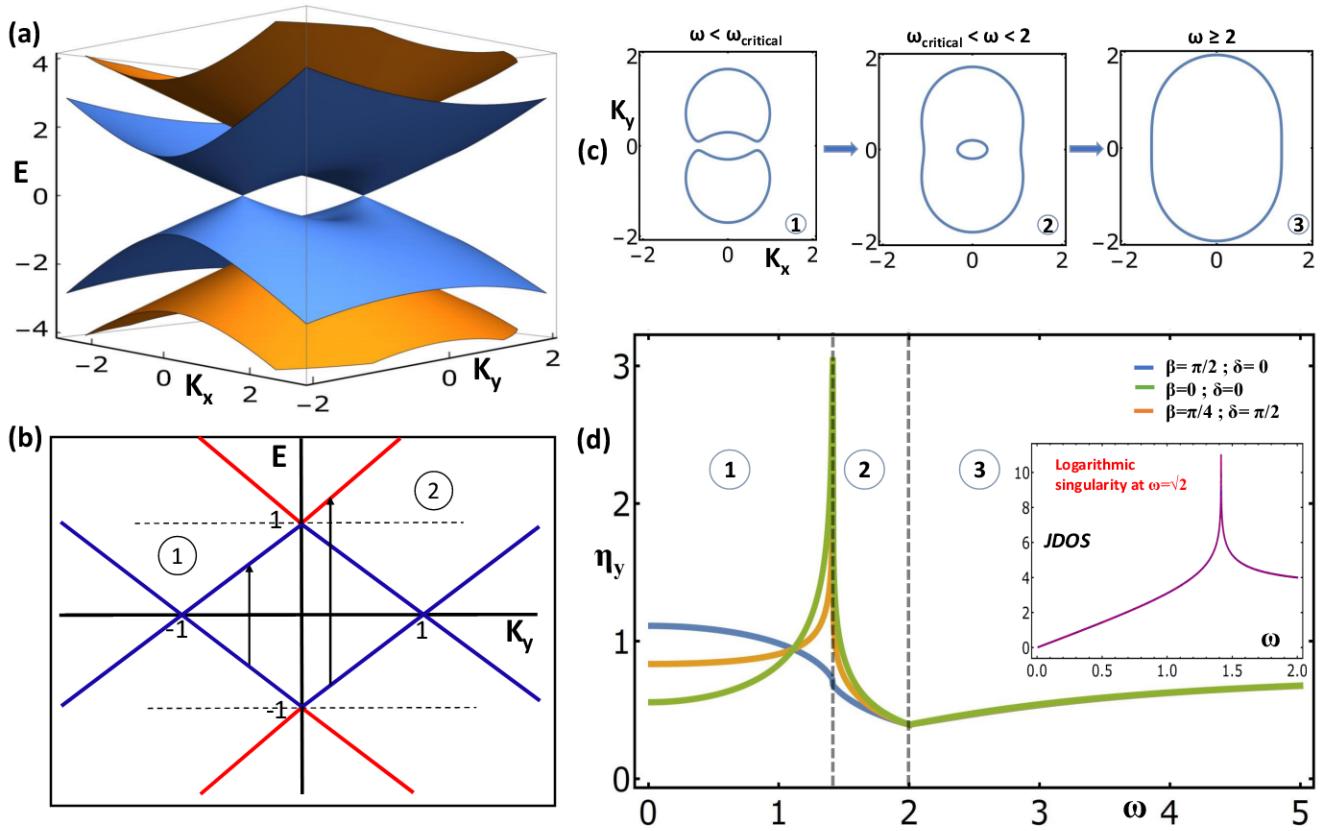
13

Figure 4: **(a)** Plot of the energy bands for magnetic field along the $y$-direction for the $\bar{X}_1$ valley. There is no gap for transitions from $v_1$ to $c_1$, as these two bands touch at the Dirac points $(0, \pm B/v)$. On the other hand, the $v_2$ and $c_2$ bands are separated by a gap $2B$ at $(0,0)$. **(b)** Plot of the band dispersion along the line $k_x = 0$. Notice that both "intra-valley" $(v_1 \rightarrow c_1)$ and "inter-valley" $(v_1 \rightarrow c_2)$ transitions are possible, the latter only for frequencies larger than $2B$. **(c)** Change of topology of the iso-energy contours with increasing excitation energy. The first change in topology occurs at the saddle-point frequency $\omega = 2B \sin \alpha$, the second at $\omega = 2B$. **(d)** Plot of the absorption coefficient $\eta_y$ (in units of $\eta_{\text{graphene}} = \frac{\pi e^2}{\hbar c}$.) vs. $\omega$ for $\alpha = \pi/4$. Notice the logarithmic singularity at $\omega = 2B \sin \alpha$ and the cusp at $\omega = 2B$. These features are related to the changes in the topology of the iso-energy contours shown in panel (c). Inset: joint density of states as a function of $\omega$ showing a logarithmic divergence at the saddle point $\omega = 2B \sin \alpha$, where $\alpha = \pi/4$.

we include $v_1 \rightarrow c_2$ and $v_2 \rightarrow c_2$ transitions.

The absorption spectrum has a logarithmic singularity at the saddle-point frequency $\omega = \omega_{\text{critical}} = 2B \sin \alpha$ (Fig. 4(d)). Furthermore, this singularity is prominent only for light polarized

14

along the $x$-direction ($\beta = 0, \delta = 0$).

To understand the origin of this singularity we have calculated the joint density of states (JDOS) which is defined as

$$g(\omega) = \sum_{\mathbf{k}} \delta\big(\omega - E_c(\mathbf{k}) - E_v(\mathbf{k})\big) = \frac{1}{2\pi\rho v^2} \sum_j \int_0^\infty d\bar{k}\bar{k} \int_{\phi_{\min}}^{\phi_{\max}} d\phi \frac{\delta(\bar{k} - \bar{k}_j(\phi))}{|d(E_c - E_v)(\bar{k}, \phi)/d\bar{k}|} , \quad (33)$$

In the vicinity of $\omega_{\text{critical}}$ this evaluates to

$$g(\omega) \simeq \frac{\omega}{\pi\rho v^2} \cot\alpha \ln\left|\frac{\sin\alpha}{\omega - \omega_{\text{critical}}}\right| . \quad (34)$$

Thus we see that the logarithmic singularity in the absorption spectrum for $x$-polarization reflects an underlying singularity in the JDOS. This singularity can also be understood by observing the change in the topology of the iso-energy contours which occurs at $\omega_{critical}$, as illustrated in panel (c) of Fig. 4. This effect – akin to the change of Fermi surface topology in a Lifshitz transition – is entirely induced by the magnetic field. The downward cusp in the absorption spectrum around $\omega = 2B$ can also be understood due to the vanishing of the inner iso-energy contour at this excitation frequency, as shown Fig. 4(c(2)).

It remains to be explained why the absorption spectrum does not have a logarithmic divergence at $\omega = \omega_{\text{critical}}$ when the incident light is polarized in the $y$-direction. In fact, in this case, we only observe a small downward cusp at $\omega = \omega_{\text{critical}}$. The reason for this difference becomes clear when we consider the behavior of the squared matrix elements of the current operators ($J_x$ and $J_y$) at the saddle point. The matrix element of $J_y$ vanishes at the saddle point energy, whereas the matrix element of $J_x$ remains finite. This is further discussed in the section IV of the supplementary material[12].

The scenario described in the previous paragraphs is not related to band anisotropy, which should be evident from the fact that we observed a strong polarization dependence of the absorption spectrum even though the anisotropy parameter $\rho$ was set to 1 (we have discussed the optical absorbance for the anisotropic Dirac cone and the total absorbance in the supplementary material section VI [12]). The scenario is also robust with respect to variations of the mixing angle $\alpha$: while the plots of Fig. 4 have been obtained for $\alpha = \pi/4$, we find the same qualitative behavior for other values of $\alpha$ (section V of the [12]).

## V. SUMMARY AND DISCUSSION

In this work, we have reported a detailed theoretical analysis of the photon absorption spectrum for a generic model of nonsymmorphic 2D semimetals with and without a magnetic field. In the absence of a magnetic field, the absorption coefficient is very similar to the absorption coefficient for graphene, which is $\frac{\pi e^2}{\hbar c} = 2.3\%$ but multiplied by the *birefringence* function we define in Eq. (24). For a strongly anisotropic cone with $\rho \ll 1$, $f(\rho, \beta)$ grows as $1/\rho$, which leads to an order of magnitude enhancement of the absorption coefficient for the anisotropic valley. Furthermore, this enhancement is highly sensitive to the direction of the photon polarization, as can be seen from the $\sin^2 \beta$ factor in the *birefringence* function. This function together with the photon polarization can enable a valley selection in absorbance spectrum in the case that a nearly isotropic valley and a strongly anisotropic valley are present near the Fermi level.

Upon switching on the magnetic field, the absorption spectrum becomes frequency-dependent, and the absorption function is also coupled with anisotropy factor $\rho$ and the mixing angle $\alpha$. We now have more than one control parameter at hand to tune the absorption coefficient, which enables us to tune the absorption coefficient efficiently by varying the photon polarization angle $\beta$. The range of tunability of the total absorbance (taking both isotropic and anisotropic valley into account) is quite broad, going from 1 to up to 10 in units of $\eta_{graphene}$, which is larger than that envisaged in previous works [21, 22]. A magnetic field perpendicular to the plane opens a gap $2B \sin \alpha$, whose observation allows an experimental determination of the hidden "mixing angle" $\alpha$. On the other hand, an in-plane magnetic field leaves the system gapless but splits the Dirac cones and makes absorption more sensitive to photon energy. For example, in Fig. 4(d), we plotted the absorption coefficient for a magnetic field along the $y$-direction as a function of frequency for different photon polarizations. The Van Hove singularity in the joint density of states, from the saddle point in the band dispersion [23], gives rise to a sharp peak in the absorption spectrum and thus greatly enhances the photon absorption at the critical frequency.

We note that the generic band model of 2D Dirac semimetals is employed in this work, and thus the results can be applied to study the optical properties of all Dirac semimetals with different nonsymmorphic lattice symmetries. The significant tunability in photon absorption enabled by the band anisotropy and external magnetic fields establishes nonsymmorphic 2D Dirac semimetals as a promising platform for optoelectronic and magnetoelectronic device applications.
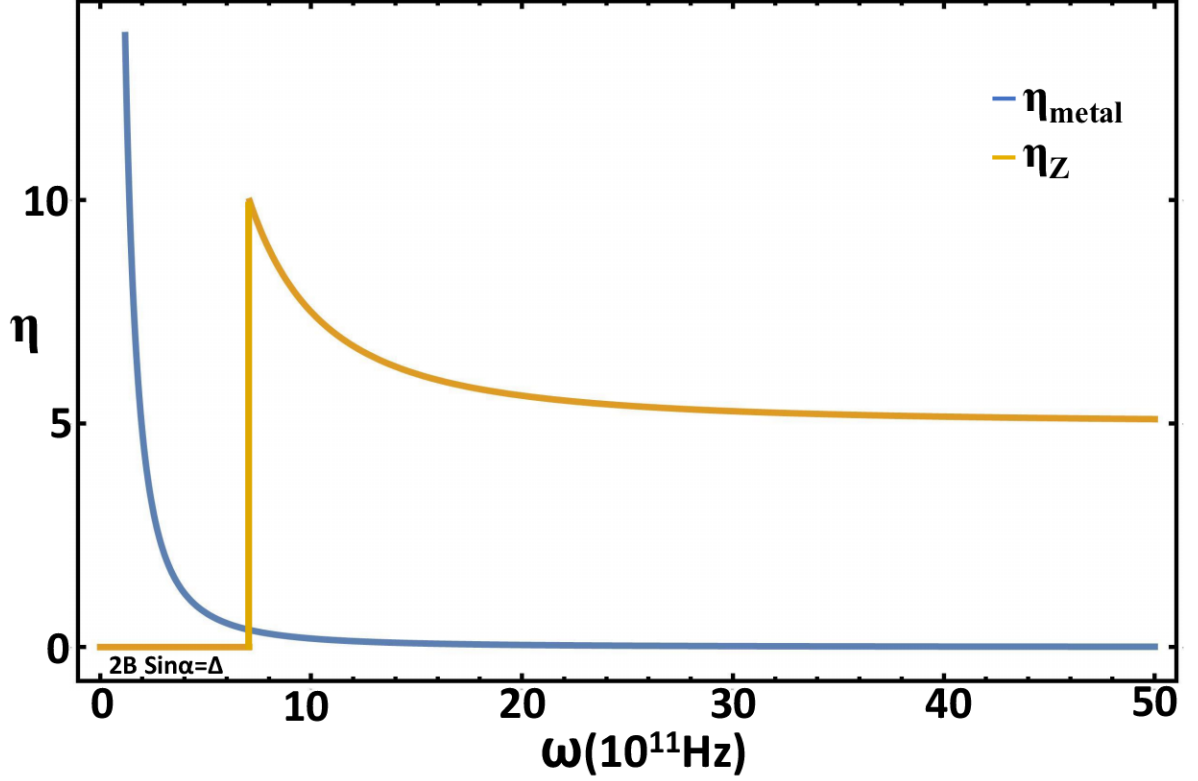
16

Figure 5: Estimated metallic absorption coefficient ($\eta_{metal}$ – blue line) vis-a-vis the absorption coefficient due to the Dirac cone with a magnetic field $B$ perpendicular to plane ($\eta_z$ – orange line) vs. frequency ($\omega$ – in units of $10^{11}$ Hz.). Our estimate of metallic absorption is based on the Drude formula for metallic conductivity, with Fermi energy on the order of 0.1 eV and momentum relaxation time $\tau = 10^{-10}s$. We also take B= 5 T and $\alpha = \pi/4$. For this very clean system the metallic absorption is a Lorentzian with a finite and sharp peak. It is well separated from the Dirac-cone absorption and the latter can be measured with negligible contribution from the former. The absorption coefficient is in units of $\frac{\pi e^2}{\hbar c} \simeq 0.023$.

We conclude with a few comments on the prospects of observing the features described in this paper in experiments on realistic materials such as $\alpha$-bismuthene. We have already mentioned the problem of positioning the symmetry-protected Dirac cone at the Fermi level, or, at least, very close to it. This can be achieved by doping or by the application of mechanical stress. However, the proper positioning of the Dirac point is not sufficient to guarantee that the low-frequency portion of the optical absorption spectrum will be dominated by interband transitions between

17

the lower and the upper Dirac cone. The reason is that, in general, there are partially occupied bands giving rise to a low-frequency metallic absorption background, which can obscure the signal from the Dirac cone. What saves the day is the fact that, in a sufficiently clean system, this background absorption (arising from intraband transitions within the partially occupied bands) has the form of a Drude peak at zero frequency with a width given by the inverse of the momentum relaxation time $\tau$. The bandgap for magnetic field in the $z$-direction is $2B\sin\alpha$, and the photon absorption from interband transition starts above the gap. Assuming a magnetic field of 1 Tesla ($\approx 10^{-23}$Joules) the width of the Drude peak becomes smaller than the gap for $\tau$ greater than $\approx 10^{-11}s$.

The Drude contribution to the absorption coefficient is calculated by dividing the power dissipated in the layer per unit area, $W_o = Re(j.E) = Re(\sigma)E^2$, where $j = \sigma E$ is the current density and $\sigma$ is the Drude conductivity of the carriers in the partially filled band, by the incident power $W_i = cE^2/(4\pi)$. The result is

$$\eta_{metallic} = \frac{W_0}{W_i} = \frac{4\pi Re(\sigma)}{c} \ . \tag{35}$$

Inserting the well-know expression for the Drude-conductivity of a two-dimensional electron gas, $\sigma = \frac{\sigma_0}{1-i\omega\tau}$, where $\sigma_0 = \frac{ne^2\tau}{m}$ and $n = \frac{m\epsilon_F}{\pi\hbar^2}$ is the two-dimensional carrier density and $\epsilon_F$ is the Fermi energy, we arrive at

$$\eta_{metallic} = \frac{\pi e^2}{\hbar c}\frac{4\epsilon_F\tau/\pi\hbar}{1 + (\omega\tau)^2} \ . \tag{36}$$

This absorption spectrum is plotted in Fig.5 vis-a-vis the one from the Dirac cone ($\eta_Z$). We have assumed a relaxation time $\tau = 10^{-10}s$, a Fermi energy of 0.1 eV, and a magnetic field of 5 T, which leads to a peak width at half maximum of about ($\mathcal{FWHM} = \frac{2\hbar}{\tau}$) 0.36 Tesla which is significantly smaller than the energy scale ($2B\sin\alpha \approx 7T$) on which the most interesting features of our nonsymmorphic model (for example, the magnetic field-induced van Hove singularity) appear. Notice that the metallic absorption spectrum is in the form of a Lorentzian ($\frac{A}{\pi}\frac{\tau}{(1+(\omega\tau)^2)}$), thus the absorption coefficient remains finite at zero frequency. Choosing a sufficiently large relaxation time we can get the width of the Drude peak to be very narrow. Theoretical studies of two-dimensional materials have shown that large values of the momentum relaxation time are possible [24, 25]. Therefore we are hopeful that for very clean materials, it will be possible to achieve $\tau \approx 10^{-10}s$ experimentally. Thus, in sufficiently clean materials the spectral features

predicted in this paper can be clearly distinguished from the Drude peak arising from the partially occupied bands.

## ACKNOWLEDGEMENTS

[1] K. S. Novoselov, A. K. Geim, S. V. Morozov, D. Jiang, M. I. Katsnelson, I. V. Grigorieva, S. V. Dubonos, and A. A. Firsov, Nature **438**, 197 (2005).

[2] M. Z. Hasan and C. L. Kane, Rev. Mod. Phys. **82**, 3045 (2010).

[3] S. M. Young, S. Zaheer, J. C. Y. Teo, C. L. Kane, E. J. Mele, and A. M. Rappe, Phys. Rev. Lett. **108**, 140405 (2012).

[4] B. Yan and C. Felser, Annual Review of Condensed Matter Physics **8**, 337 (2017), https://doi.org/10.1146/annurev-conmatphys-031016-025458.

[5] N. Nagaosa, T. Morimoto, and Y. Tokura, Nature Reviews Materials **5**, 621 (2020).

[6] S. Cahangirov, M. Topsakal, E. Aktürk, H. Şahin, and S. Ciraci, Phys. Rev. Lett. **102**, 236804 (2009).

[7] P. Vogt, P. De Padova, C. Quaresima, J. Avila, E. Frantzeskakis, M. C. Asensio, A. Resta, B. Ealet, and G. Le Lay, Phys. Rev. Lett. **108**, 155501 (2012).

[8] S. Z. Butler, S. M. Hollen, L. Cao, Y. Cui, J. A. Gupta, H. R. Gutiérrez, T. F. Heinz, S. S. Hong, J. Huang, A. F. Ismach, E. Johnston-Halperin, M. Kuno, V. V. Plashnitsa, R. D. Robinson, R. S. Ruoff, S. Salahuddin, J. Shan, L. Shi, M. G. Spencer, M. Terrones, W. Windl, and J. E. Goldberger, ACS Nano **7**, 2898 (2013), pMID: 23464873, https://doi.org/10.1021/nn400280c.

[9] H. Liu, A. T. Neal, Z. Zhu, Z. Luo, X. Xu, D. Tománek, and P. D. Ye, ACS Nano **8**, 4033 (2014), pMID: 24655084, https://doi.org/10.1021/nn501226z.

[10] S. M. Young and C. L. Kane, Phys. Rev. Lett. **115**, 126803 (2015).

[11] P. J. Kowalczyk, S. A. Brown, T. Maerkl, Q. Lu, C.-K. Chiu, Y. Liu, S. A. Yang, X. Wang, I. Zasada, F. Genuzio, T. O. MenteÅŸ, A. Locatelli, T.-C. Chiang, and G. Bian, ACS Nano **14**, 1888 (2020),

pMID: 31971774, https://doi.org/10.1021/acsnano.9b08136.

[12] See Supplemental Material at (URL will be inserted by publisher) to have detailed analysis on our formalism.

[13] S. Deng, L. Li, and Y. Zhang, ACS Applied Nano Materials **1**, 1932 (2018), https://doi.org/10.1021/acsanm.8b00363.

[14] L. Xu, W.-Q. Huang, W. Hu, K. Yang, B.-X. Zhou, A. Pan, and G.-F. Huang, Chemistry of Materials **29**, 5504 (2017), https://doi.org/10.1021/acs.chemmater.7b00281.

[15] X. Zhao, B. Qiu, W. Yue, G. Hu, J. Ren, and X. Yuan, The European Physical Journal B **92**, 44 (2019).

[16] J. Cui, Z. Zhang, D. Liu, D. Zhang, W. Hu, L. Zou, Y. Lu, C. Zhang, H. Lu, C. Tang, N. Jiang, I. P. Parkin, and D. Guo, Nano Letters **19**, 6569 (2019), pMID: 31381357, https://doi.org/10.1021/acs.nanolett.9b02821.

[17] S. Guan, Y. Liu, Z.-M. Yu, S.-S. Wang, Y. Yao, and S. A. Yang, Phys. Rev. Materials **1**, 054003 (2017).

[18] K.-H. Jin, H. Huang, Z. Wang, and F. Liu, Nanoscale **11**, 7256 (2019).

[19] R. Huang, J. Li, Z. Wu, W. Yang, W. Huang, C. Li, and S. Chen, Physics Letters A **382**, 3035 (2018).

[20] M. I. Katsnelson, Graphene: Carbon in Two Dimensions (Cambridge University Press, 2012).

[21] A. Kumar, G. Sachdeva, R. Pandey, and S. P. Karna, Applied Physics Letters **116**, 263102 (2020), https://doi.org/10.1063/5.0010794.

[22] T. Jiang, D. Huang, J. Cheng, X. Fan, Z. Zhang, Y. Shan, Y. Yi, Y. Dai, L. Shi, K. Liu, C. Zeng, J. Zi, J. E. Sipe, Y.-R. Shen, W.-T. Liu, and S. Wu, Nature Photonics **12**, 430 (2018).

[23] L. Van Hove, Phys. Rev. **89**, 1189 (1953).

[24] E. H. Hwang and S. Das Sarma, Phys. Rev. B **77**, 195412 (2008).

[25] Y. Zhan, "Two distinct methods to evaluate graphene relaxation time and mobility in boltzmann diffusive transport, considering ionized impurity scattering and thomas-fermi screening," (2017), arXiv:1712.08965 [cond-mat.mes-hall].